Supporting Information

Cyanometallic Charge Engineering in Spin Crossover Metal-Organic Frameworks

Bang-Heng Lyu,[†] Kai-Ping Xie,[†] Wen Cui, Yan-Cong Chen, Guan-Xi Chen, Si-Guo Wu[*] and Ming-Liang Tong[*]

Key Laboratory of Bioinorganic and Synthetic Chemistry of Ministry of Education, School of Chemistry, IGCME, GBRCE for Functional Molecular Engineering, Sun Yat-Sen University, Guangzhou 510275 (P. R. China)
E-mail: wusg6@mail.sysu.edu.cn; tongml@mail.sysu.edu.cn.

Contents

Experimental Procedures 3

Crystal Data and Structures.....5

Powder X-Ray Diffraction 14

Thermogravimetric Analysis.....17

Infrared spectra 21

XPS Measurements 23

EDS Measurements.....24

Mass spectrum.....25

Magnetization.....26

Referrence 35

Experimental Procedures

Materials and methods

All the reagents and solvents were commercially available and used without further purification. Elemental analyses of C, H and N were carried out with an Elementar Vario-EL CHNS elemental analyzer. Thermogravimetric analyses (TGA) were performed on a TA Instrument NETZSCH TG 209 F3 or NETZSCH TG 209 F1 Libra under a nitrogen flow atmosphere at a heating rate of 10 K min^{-1}. FT-IR spectra were recorded on Thermo Scientific Nicolet 6700-Contiuum instrument in KBr tablets in the range of 4000~400 cm^{-1}. X-ray photoelectron spectroscopy (XPS) measurements were performed on a Thermo Fisher Scientific ESCALAB Xi+ system using an Al-K_α source. Elemental composition analyses were measured using a Quanta 400F thermal field emission scanning electron microscope (SEM) equipped with an energy dispersive X-ray spectrometer (EDS) attachment. Electrospray mass spectra were recorded on a ThermoFisher LSQ XL instrument. Powder X-ray diffraction (PXRD) patterns were obtained on a Rigaku Smartlab X-ray diffractometer (Cu-K_α, λ = 1.54056 Å) in capillary test mode at room temperature. Differential Scanning Calorimetry (DSC) was performed on a NETZSCH DSC 200 F3 with a sweeping rate of 10 K min^{-1} under N_2 atmosphere.

Synthesis procedure

[Fe(TPPE){Au(CN)$_2$}]Br·4H$_2$O·8TCE (**1**): K[Au(CN)$_2$]·2H$_2$O (0.025 mmol) and TPPE (0.025 mmol) were dissolved in 4.5 mL of TCE/MeOH solution (v:v = 2:1) and placed in the bottom of a test tube. Then, 9 mL of TCE/MeOH solution (v:v = 1:1) was carefully added as the buffer solution, followed by 2.5 mL of methanol solution of $FeBr_2$ (0.025 mmol) at the top. Yellow block crystals suitable for single crystal X-ray measurement were obtained after 2 weeks. Yield: 74.4%. Anal. calcd for $C_{64}H_{56}N_6Cl_{32}FeBrAuO_4$: C, 31.50; H, 2.31; N, 3.44. Found: C, 31.33; H, 2.14; N, 3.77.

[Fe(TPPE){Fe(CN)$_5$NO}]·7H$_2$O·6DEF·EtOH (**2**): Na$_2$[Fe(CN)$_5$NO]·2H$_2$O (0.0125 mmol) and TPPE (0.0125 mmol) were dissolved in 4.5 mL of DEF/EtOH solution (v:v = 2:1) and placed in the bottom of a test tube. Then, 10 mL of DEF/EtOH solution (v:v = 1:1) was carefully added as the buffer solution, followed by 1.5 mL of ethanol solution of Fe(ClO$_4$)$_2$·6H$_2$O (0.0125 mmol) at the top. Red brown block crystals suitable for single crystal X-ray measurement were obtained after 2 weeks. Yield: 51.7%. Anal. calcd for $C_{83}H_{118}Fe_2N_{16}O_{15}$: C, 58.93; H, 7.03; N, 13.25. Found: C, 59.00; H, 6.88; N, 13.14.

(PPN)$_3$[Co(CN)$_6$]: The complexes were prepared by mixing saturated H$_2$O/MeOH (v:v = 3:1) solutions of K$_3$[Co(CN)$_6$] and PPNCl (bis(triphenylphosphine)iminium chloride).[1] The white precipitates were isolated by filtration, washed with the mixed solvent and then dried at room temperature over silica gel.

(Et$_2$NH$_2$)[Fe(TPPE){Co(CN)$_6$}]·11H$_2$O·6DEF·2MeOH (**3**): PPN$_3$[Co(CN)$_6$] (0.0125 mmol) and TPPE (0.0125 mmol) were dissolved in 4.5 mL of DEF/MeOH solution (v:v = 3:1) and placed in the bottom of a test tube. Then, 10 mL of DEF/MeOH solution (v:v = 2:1) was carefully added as the buffer solution, followed by 1.5 mL of methanol solution of Fe(ClO$_4$)$_2$·6H$_2$O (0.0125 mmol) at the top. Yellow block solvated crystals **3** suitable for single crystal X-ray measurement were obtained after 5 weeks. Yield: 18.9%. Anal. calcd for $C_{88}H_{140}N_{17}FeCoO_{19}$: C, 56.98; H, 7.61; N, 12.84. Found: C, 57.26; H, 7.34; N, 12.87.

(Et$_2$NH$_2$)[Fe(TPPE){Co(CN)$_6$}]·*solv* (**3′**): Partial desolvated species **3′** was obtained by heating **3** at 338 K under a N_2 atmosphere for half hour. This compound retained poor crystallinity but was found to be still suitable for PXRD studies. **3′** is air-sensitive and will reabsorb moisture from the air, which leads to uncertain solvent compositions. Attempt to prepared the fully desolvated sample by heating at 200°C under N_2 atmosphere, however, the empty

framework collapsed as all the solvents escaped from the lattice (Figure S26).

X-ray Crystallography

The single crystal of **1**–**3** ware sealed in capillary containing mother liquor for variable temperature structural determination. Variable temperature single crystal X-ray diffraction data of complexes **1**–**2** were collected on a Bruker D8 QUEST diffractometer with Mo-K_α radiation (λ = 0.71073 Å). For complex **3**, high temperature single crystal X-ray data were recorded on a Bruker D8 VENTURE with Ga-K_α radiation (λ = 1.34138 Å). All the data indexing and integration were carried out with Bruker Smart program. The structures were solved by intrinsic phasing methods and all non-hydrogen atoms were refined with anisotropic displacement parameters by least-squares on F^2 values using SHELXL program in OLEX2.[2-4] The hydrogen atoms were refined using a riding model. The solvents in the lattice of **1**–**3** are highly disordered and were omitted by using solvent mask process in OLEX2. Responses to checkCIF alerts are quoted in the validation response form. Crystallographic data for this paper can be obtained from the Cambridge Crystallographic Data Centre (CCDC) with deposited numbers of 2325159(1-91 K), 2325160(1-255 K), 2325161(2-120 K), 2325162(2-298 K), 2325164(3-293 K).

Magnetic susceptibility measurements

Variable temperature magnetic susceptibilities of polycrystalline samples were measured on a Quantum Design MPMS3 SQUID magnetometer under an applied field of 5 kOe with a sweeping rate of 2 K min^{-1}. Polycrystalline samples **1**–**3** were embedded in plastic film with a small amount of mother liquor. Magnetic susceptibilities of partially desolvated sample **3**′ was measured without mother liquor. Diamagnetic contribution was performed based on Pascal's constants.

Crystal Data and Structures

Table S1. Crystallographic data for **1**.

Empirical formula	$C_{64}Cl_{32}FeAuBrH_{56}N_6O_4$	
Formula weight	2440.27	
Temperature / K	91	255
Crystal system	orthorhombic	
Space group	*Cmmm*	*Pmmm*
a / Å	20.0212(8)	10.4824(5)
b / Å	28.7967(13)	14.6177(9)
c / Å	16.6677(7)	17.0399(9)
α / °	90	90
β / °	90	90
γ / °	90	90
V / Å^3	9609.7(7)	2611.0(2)
Z	4	1
ρ_{calc} g/cm^3	1.687	1.552
μ / mm^{-1}	3.026	2.785
F(000)	4792.0	1198.0
Crystal size / mm^3	0.261 × 0.192 × 0.155	0.261 × 0.192 × 0.155
Radiation	Mo-K_α (λ = 0.71073)	Mo-K_α (λ = 0.71073)
Reflections collected	50587	26797
Independent reflections	6171	3502
Goodness-of-fit on F^2	1.079	1.161
Final R indexes [I>=2σ (I)]	R_1 = 0.0552, wR_2 = 0.1620	R_1 = 0.0969, wR_2 = 0.2642
Final R indexes [all data]	R_1 = 0.0588, wR_2 = 0.1641	R_1 = 0.1056, wR_2 = 0.2725
Largest diff. peak/hole / e Å^{-3}	3.08/−1.76	4.94/−1.54
CCDC	2325159	2325160

$^a R_1 = \Sigma|F_o| - |F_c||/\Sigma|F_o|$; $^b wR_2 = \{[\Sigma w(F_o^2-F_c^2)^2]/\Sigma[w(F_o^2)^2]\}^{1/2}$

Table S2. Crystallographic data for **2**.

Empirical formula	$C_{83}Fe_2H_{118}N_{16}O_{15}$	
Formula weight	1691.63	
Temperature / K	120	298
Crystal system	orthorhombic	
Space group	*Cmmm*	
a / Å	19.818(2)	20.623(2)
b / Å	29.050(3)	29.230(3)
c / Å	16.4847(18)	17.010(2)
α / °	90	90
β / °	90	90
γ / °	90	90
V / Å^3	9490.4(18)	10254(2)
Z	4	4
ρ_{calc} g/cm^3	1.184	1.096
μ / mm^{-1}	0.371	0.344
F(000)	3600.0	3600.0
Crystal size / mm^3	0.191 × 0.14 × 0.131	0.322 × 0.221 × 0.194
Radiation	Mo-K_α (λ = 0.71073)	Mo-K_α (λ = 0.71073)
Reflections collected	37621	48274
Independent reflections	6128	4954
Goodness-of-fit on F^2	1.105	1.087
Final R indexes [I>=2σ (I)]	R_1 = 0.0778, wR_2 = 0.2378	R_1 = 0.1184, wR_2 = 0.2564
Final R indexes [all data]	R_1 = 0.1093, wR_2 = 0.2545	R_1 = 0.1400, wR_2 = 0.2682
Largest diff. peak/hole / e Å^{-3}	1.12/−0.67	0.99/−0.61
CCDC	2325161	2325162

$^a R_1 = \Sigma|F_o| - |F_c||/\Sigma|F_o|$; $^b wR_2 = \{[\Sigma w(F_o^2 - F_c^2)^2]/\Sigma[w(F_o^2)^2]\}^{1/2}$

Table S3. Crystallographic data for **3**.

	3
Empirical formula	$C_{88}CoFeH_{140}N_{17}O_{19}$
Formula weight	1854.94
Temperature / K	293
Crystal system	orthorhombic
Space group	*Pmmm*
a / Å	10.2180(8)
b / Å	14.6762(12)
c / Å	17.0726(12)
α / °	90
β / °	90
γ / °	90
V / Å^3	2560.2(3)
Z	1
ρ_{calc} g/cm^3	1.203
μ / mm^{-1}	2.017
F(000)	992.0
Crystal size / mm^3	0.14 × 0.1 × 0.08
Radiation	Ga-K_α (λ = 1.34138)
Reflections collected	27214
Independent reflections	3205
Goodness-of-fit on F^2	1.130
Final R indexes [I>=2σ (I)]	R_1 = 0.0641, wR_2 = 0.2034
Final R indexes [all data]	R_1 = 0.0769, wR_2 = 0.2159
Largest diff. peak/hole / e Å^{-3}	0.41/−0.41
CCDC	2325164

$^aR_1 = \Sigma|F_o| - |F_c||/\Sigma|F_o|$; $^bwR_2 = \{[\Sigma w(F_o^2-F_c^2)^2]/\Sigma[w(F_o^2)^2]\}^{1/2}$

Table S4. Selected bond lengths for **1**.

T / K	91	255
Fe1−N1 / Å	1.908(5)	2.118(11)
Fe1−N2 / Å	2.017(3)	2.218(5)
<Fe1−N>[a] / Å	1.981	2.185
ζFe1[b] / Å	0.292	0.266
ΣFe1[c] / °	9.19	6.79
∠N1−Fe1−N1[i] / °	180	180
∠Fe1−N1≡C1 / °	175.9(5)	180
∠Au1−C1≡N1 / °	178.6(5)	180
∠C1−Au1−C1[ii] / °	176.3(3)	180
∠Fe1…Au1…Fe1 / °	171.5	180.0

[a]average Fe−N bond length; [b]Octahedral stretching distortion parameters; [c]Octahedral angular distortion parameters; Symmetry codes: (i-91 K) 1/2-X, 3/2-Y, 2-Z; (i-255 K) -X, -Y, 1-Z; (ii-91 K) 1-X, +Y, 2-Z; (ii-255 K) 1-X, -Y, 1-Z.

Table S5. Selected bond lengths for **2**.

T / K	120	298
Fe1−N1 / Å	1.913(3)	2.115(5)
Fe1−N2 / Å	2.011(1)	2.200(4)
<Fe1−N>[a] / Å	1.978	2.172
ζFe1[b] / Å	0.259	0.223
ΣFe1[c] / °	8.13	8.97
∠N1−Fe1−N1[i] / °	180	180
∠Fe1−N1≡C1 / °	178.1(3)	176.5(5)
∠Fe2−C1≡N1 / °	178.4(4)	179.5(6)
∠C1−Fe2−C1[ii] / °	169.8(2)	172.0(4)
∠Fe1…Fe2…Fe1 / °	166.3	168.6

[a]average Fe−N bond length; [b]Octahedral stretching distortion parameters; [c]Octahedral angular distortion parameters; Symmetry codes: (i-120 K) 3/2-X, 3/2-Y, 1-Z; (i-298 K) 1/2-X, 1/2-Y, 1-Z; (ii-120 K) 1-X, +Y, 1-Z; (ii-298 K) -X, +Y, 1-Z.

Table S6. Selected bond lengths for **3**.

	3
T / K	293
Fe1−N1 / Å	2.090(4)
Fe1−N2 / Å	2.240(3)
<Fe1−N>[a] / Å	2.190
ζFe1[b] / Å	0.403
ΣFe1[c] / °	7.79
ΣCo1 / °	0.36
∠N1−Fe1−N1[i] / °	180
∠Fe1−N1≡C1 / °	180
∠Co1−C1≡N1 / °	180
∠C1−Co1−C1[ii] / °	180
∠Fe1…Co1…Fe1 / °	180.0

[a]average Fe−N bond length; [b]Octahedral stretching distortion parameters; [c]Octahedral angular distortion parameters; Symmetry codes: (i) 2-X, 1-Y, 1-Z; (ii) 1-X, 1-Y, 1-Z.

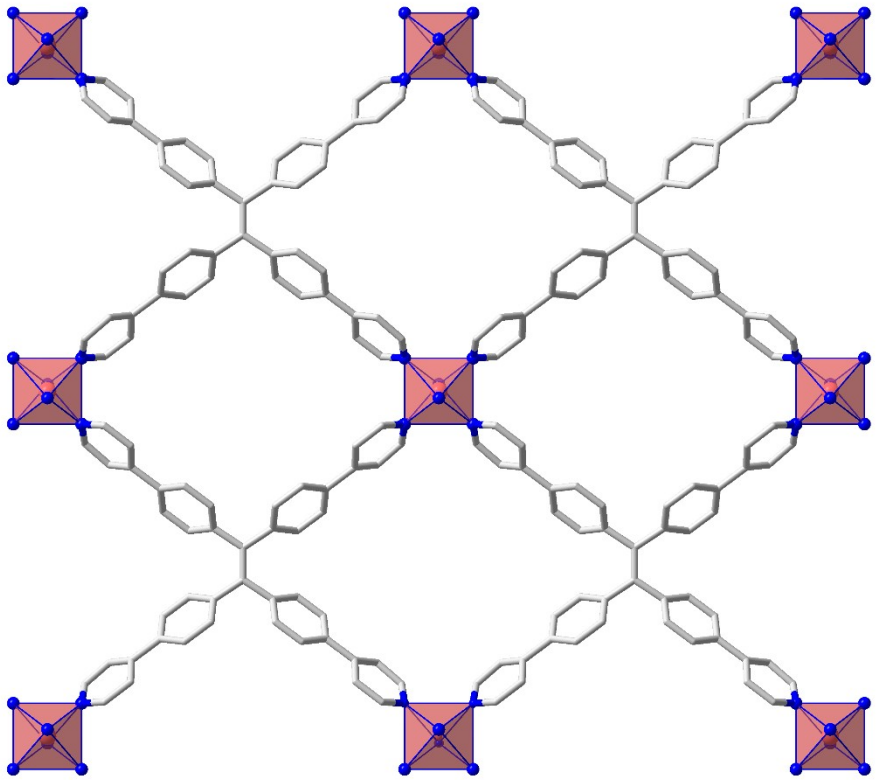

Figure S1. The 2D network of $[Fe(TPPE)]_n$.

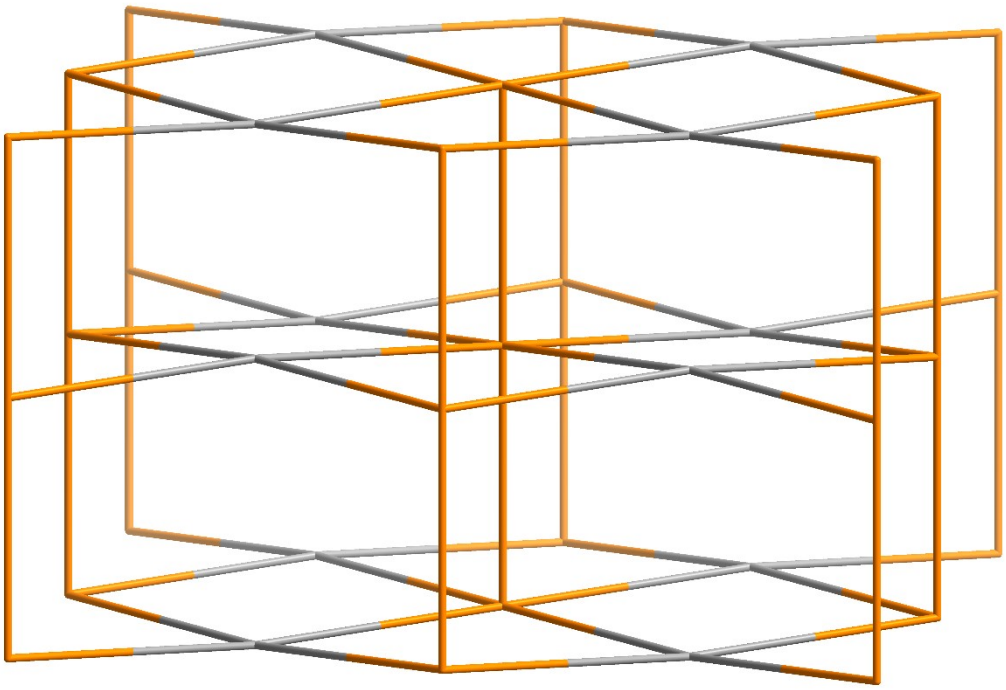

Figure S2. View of 4,6-connected net with *fsc* topology for **1**–**3**; color code: Fe, orange; simplified TPPE, gray.

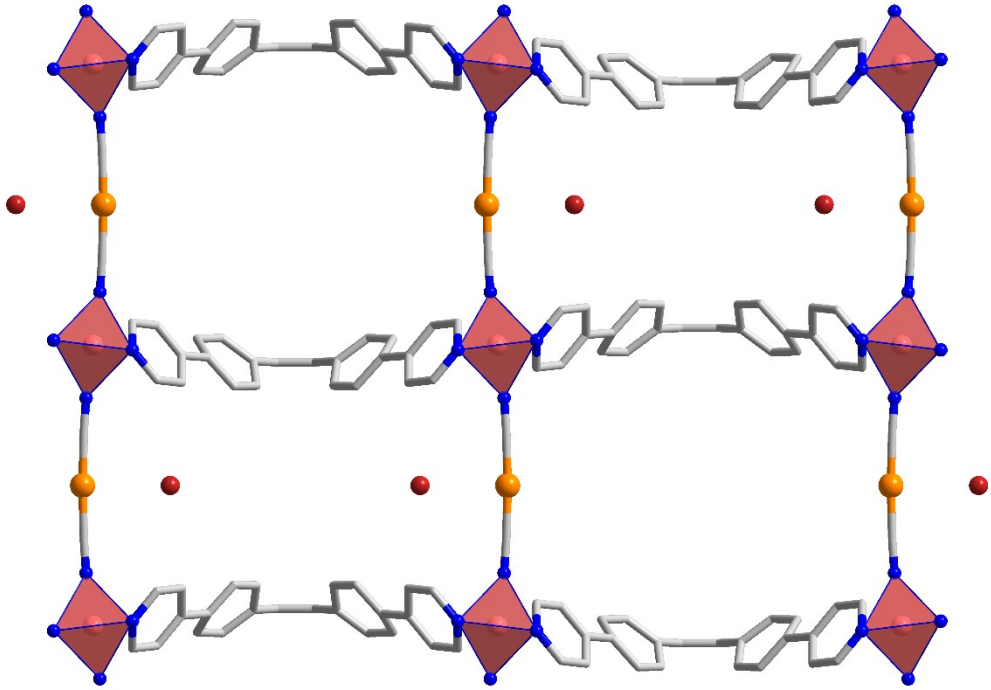

Figure S3. Packing view of **1** along the *a* axis. Color code: Fe, Pink; Au, orange; N, blue; C, grey; Br, red. The hydrogen atoms are omitted for clarity.

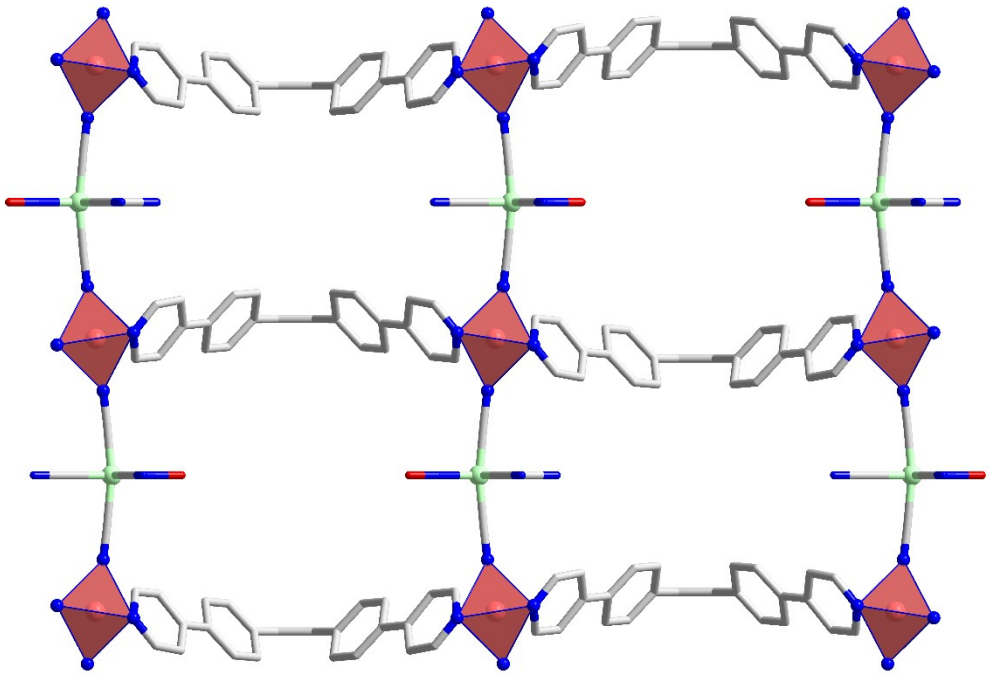

Figure S4. Packing view of **2** along the *a* axis. Color code: Fe(N6), Pink; Fe(nitroprusside), green; N, blue; C, grey; O, red. The hydrogen atoms are omitted for clarity.

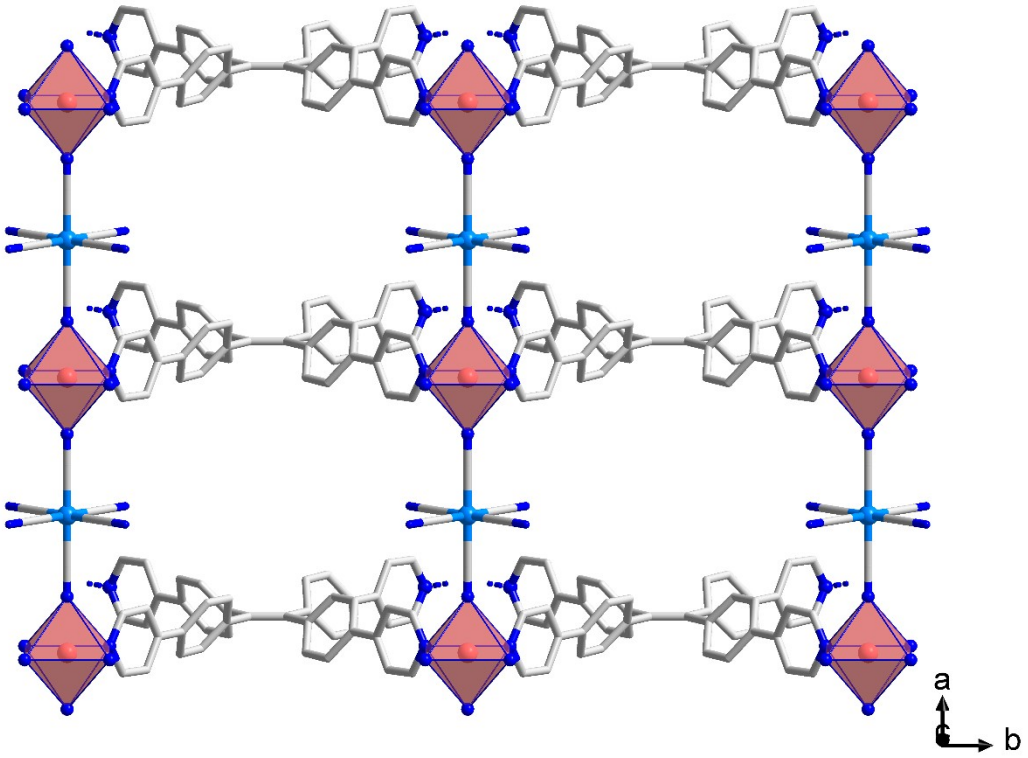

Figure S5. Packing view of **3**. Color code: Fe, Pink; Co, light blue; N, blue; C, grey. The hydrogen atoms are omitted for clarity.

Powder X-Ray Diffraction

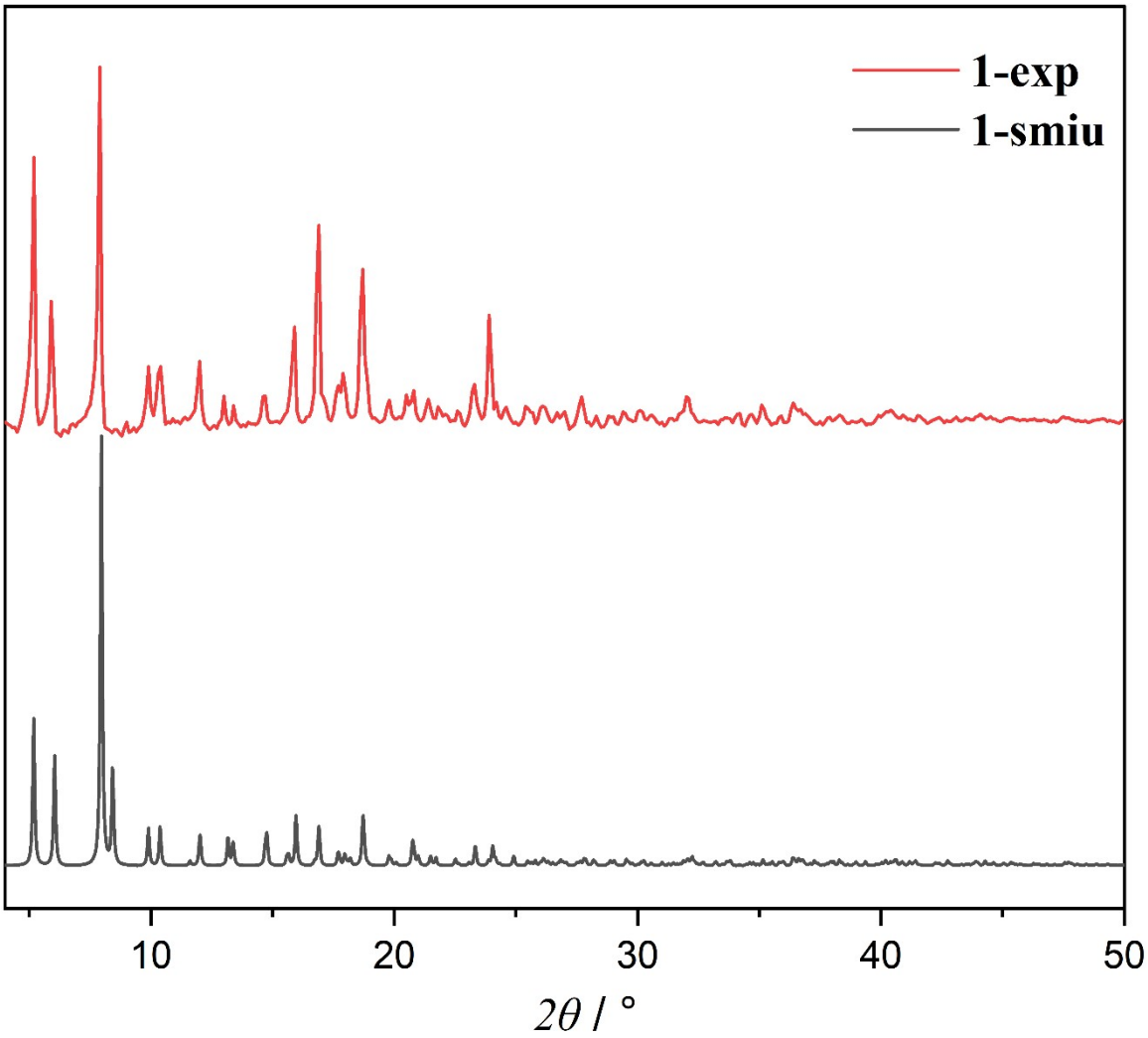

Figure S6. Powder X-ray diffraction (PXRD) patterns for **1**. The simulated PXRD pattern was obtained from crystal data at 255 K.

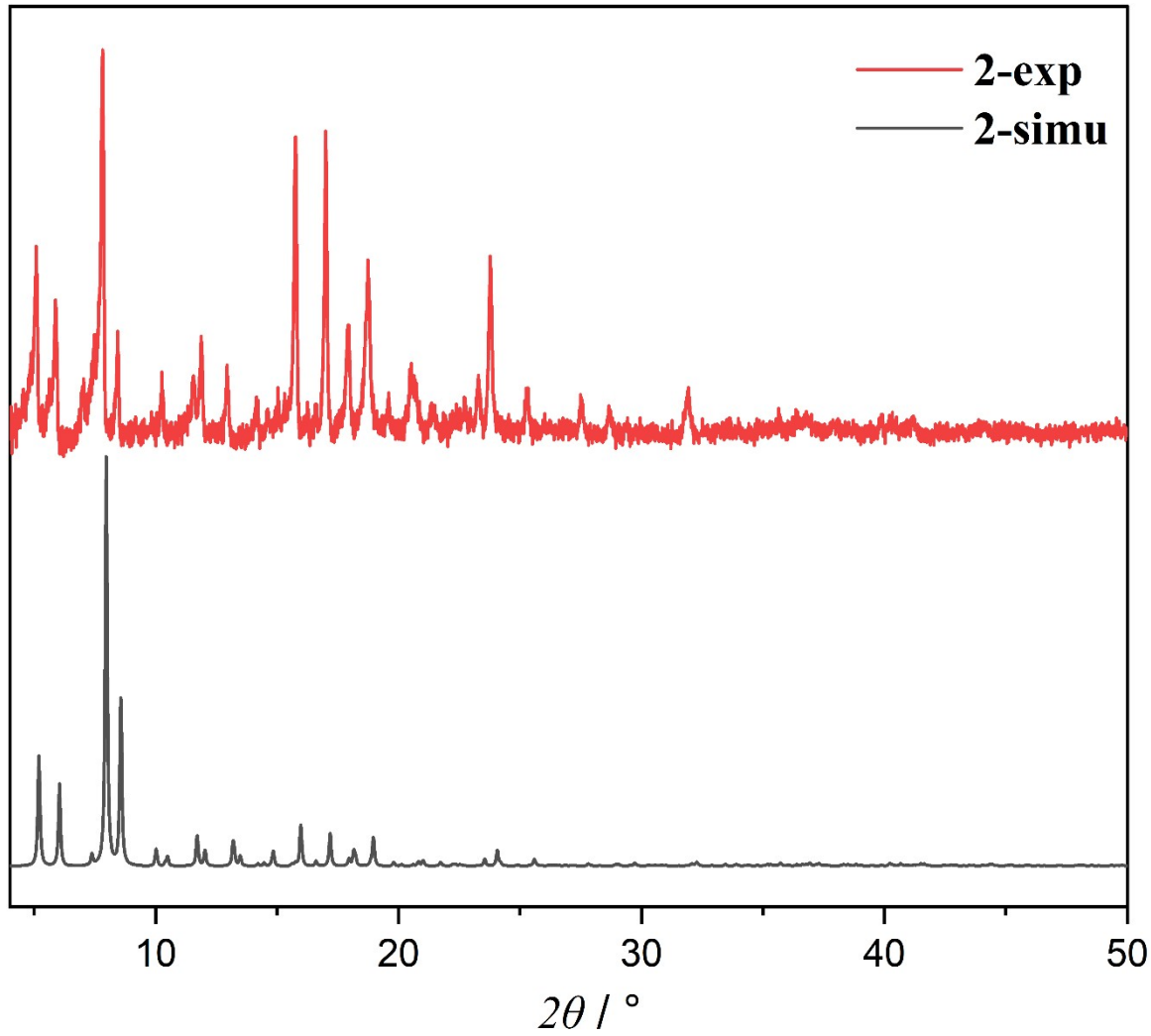

Figure S7. Powder X-ray diffraction (PXRD) patterns for **2**. The simulated PXRD pattern was obtained from crystal data at 298 K.

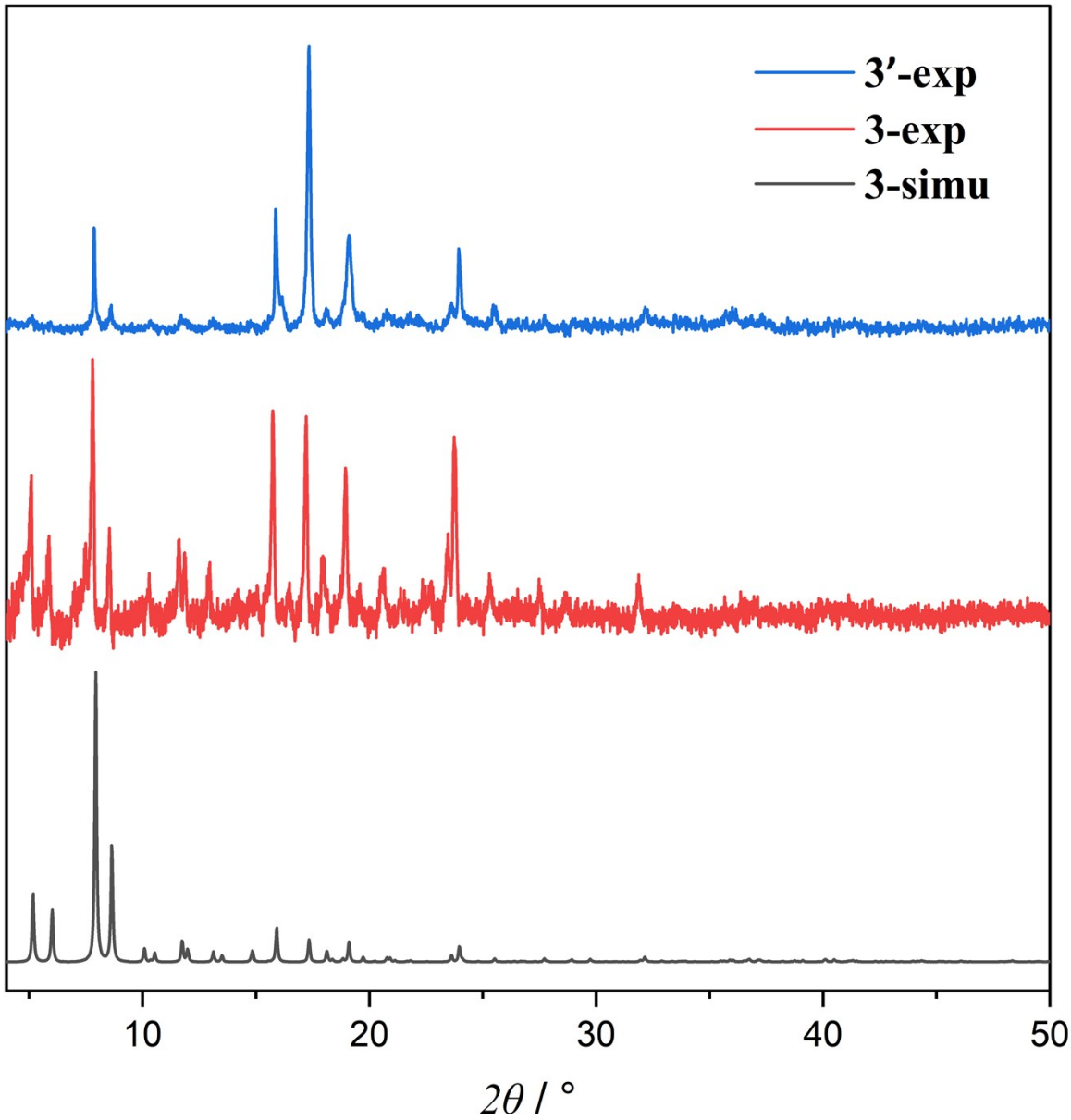

Figure S8. Powder X-ray diffraction (PXRD) patterns for **3** and **3**′.

Thermogravimetric Analysis

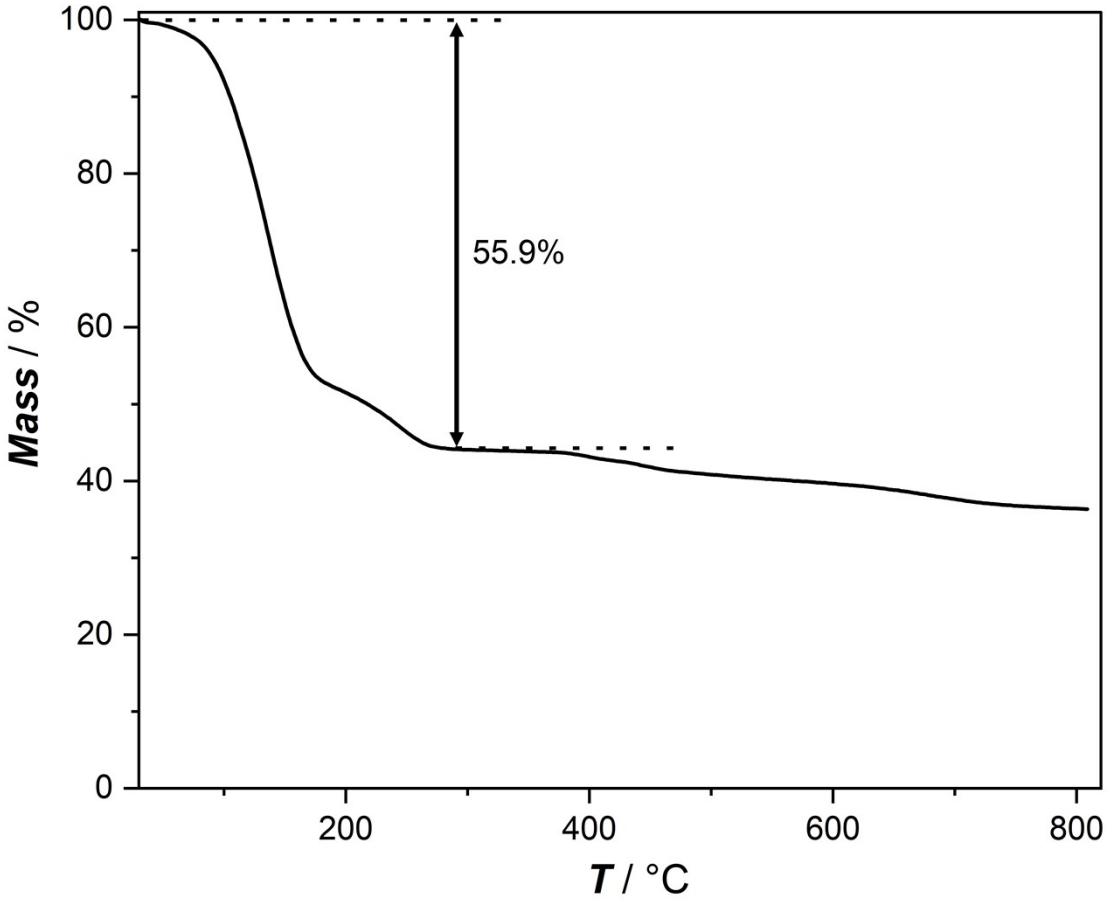

Figure S9. Thermogravimetric analysis curve of **1**. The weight loss of 55.9% is close to the theoretical value of 58% corresponding to the escape of $4H_2O$ and 8TCE molecules.

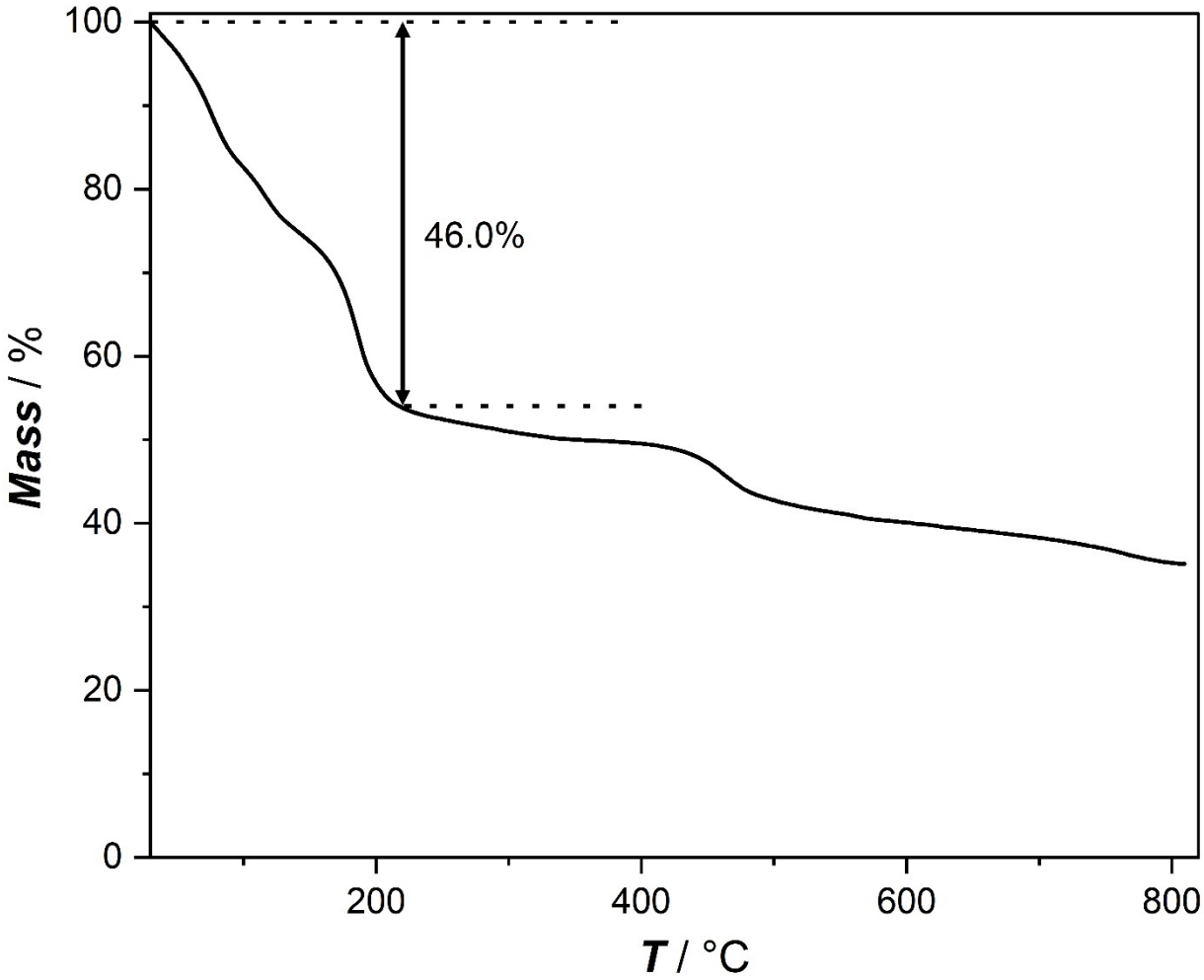

Figure S10. Thermogravimetric analysis curve of **2**. The weight loss of 46.0% is close to the theoretical value of 46.1% corresponding to the escape of $7H_2O$, 6DEF and EtOH molecules.

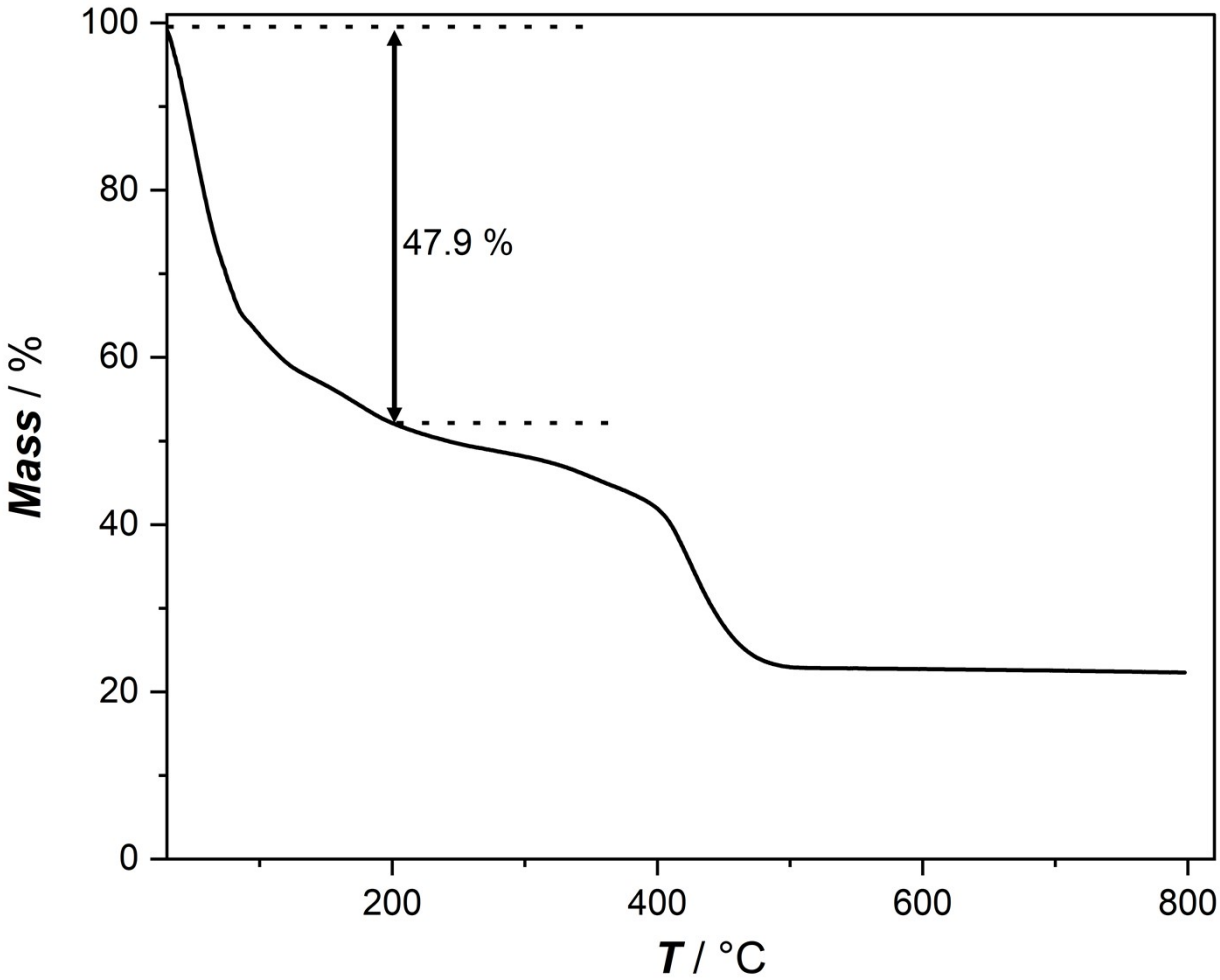

Figure S11. Thermogravimetric analysis curve of **3**. The weight loss of 47.9% is close to the theoretical value of 46.9% corresponding to the escape of $11H_2O$, 6DEF and 2MeOH molecules.

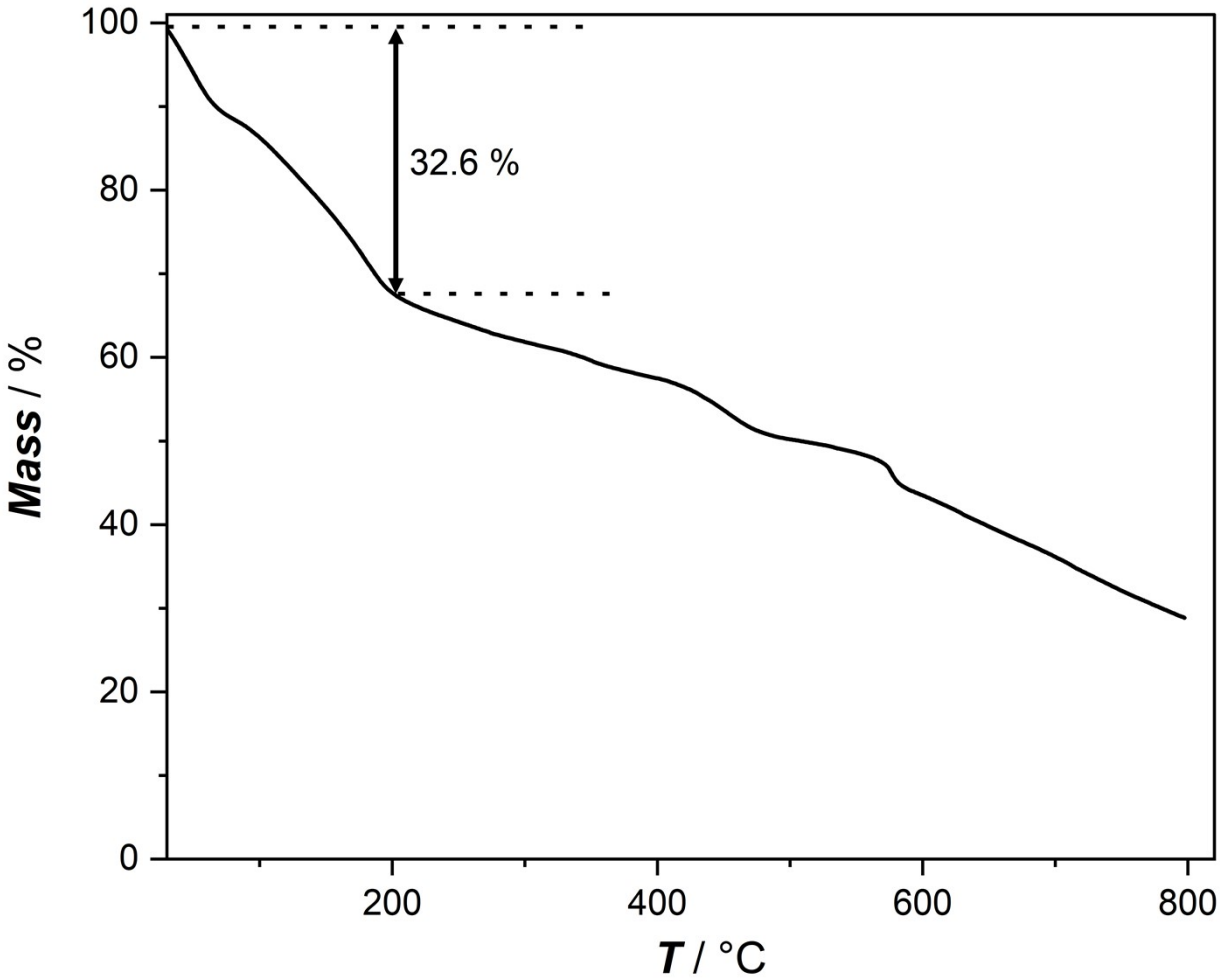

Figure S12. Thermogravimetric analysis curve of **3'**. The weight loss of 32.6% is close to the theoretical value of 32.9% corresponding to the escape of $10H_2O$ and 3DEF molecules.

Infrared spectra

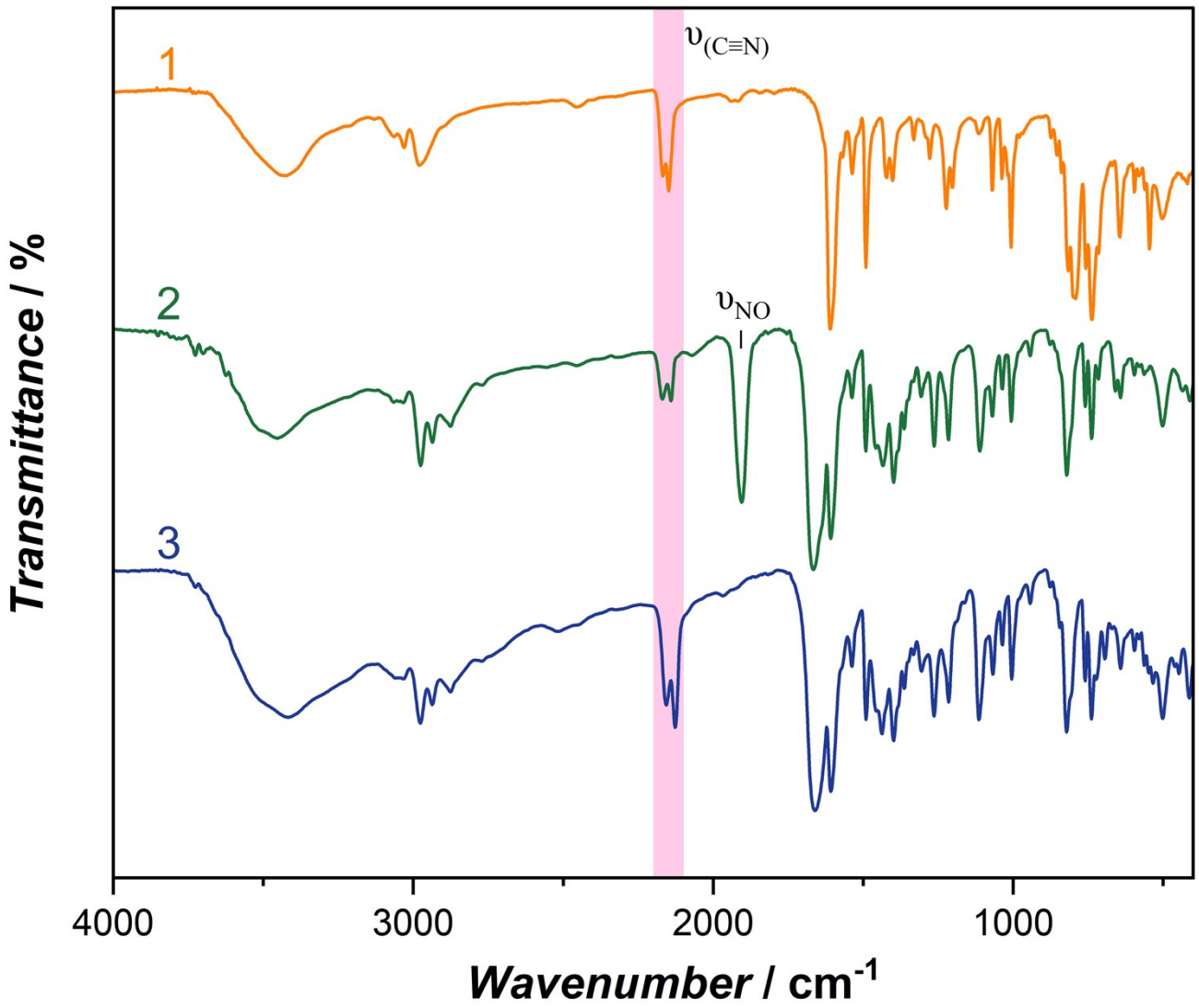

Figure S13. IR spectra of **1**–**3**.

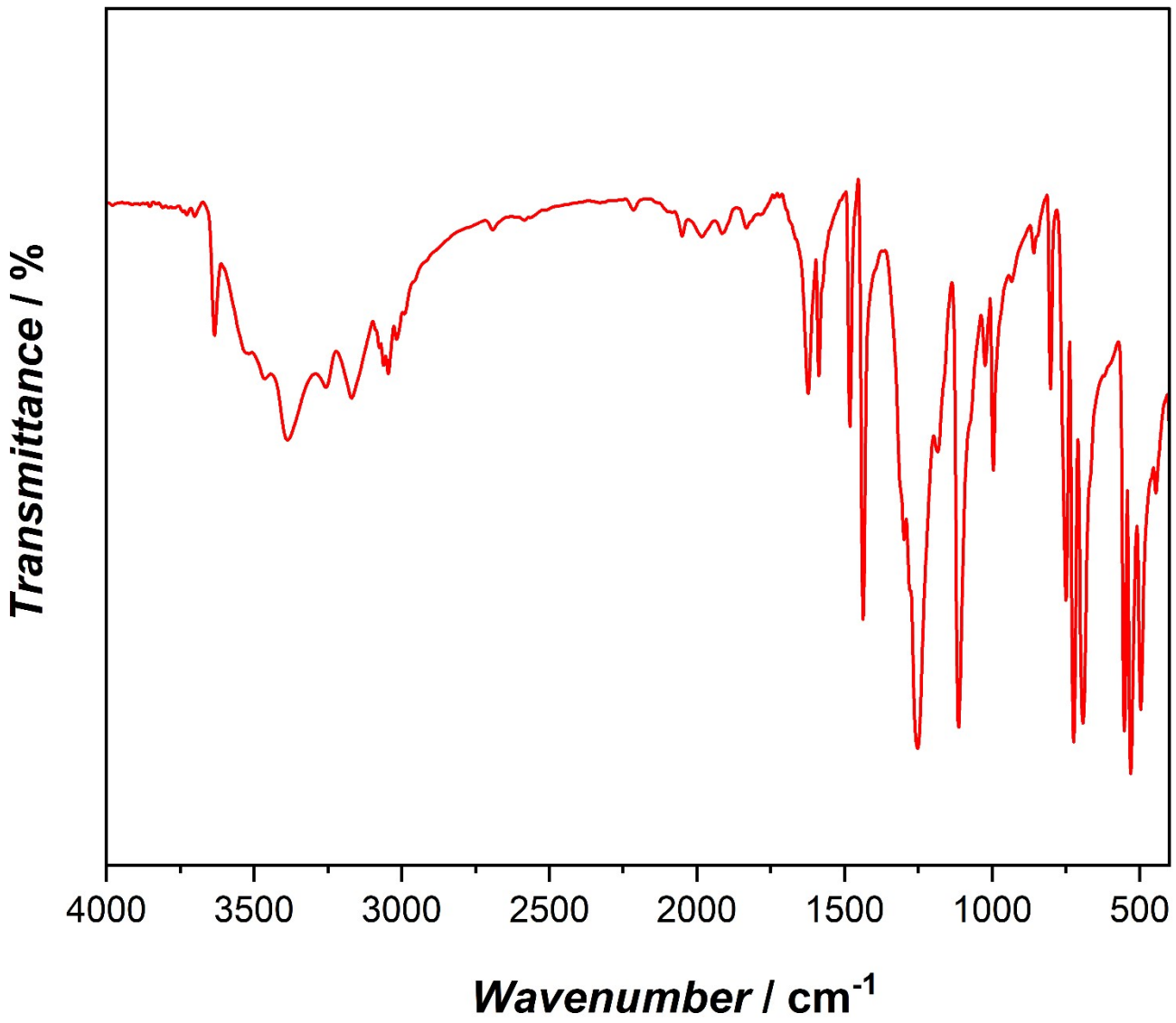

Figure S14. IR spectra of PPNCl.

XPS Measurements

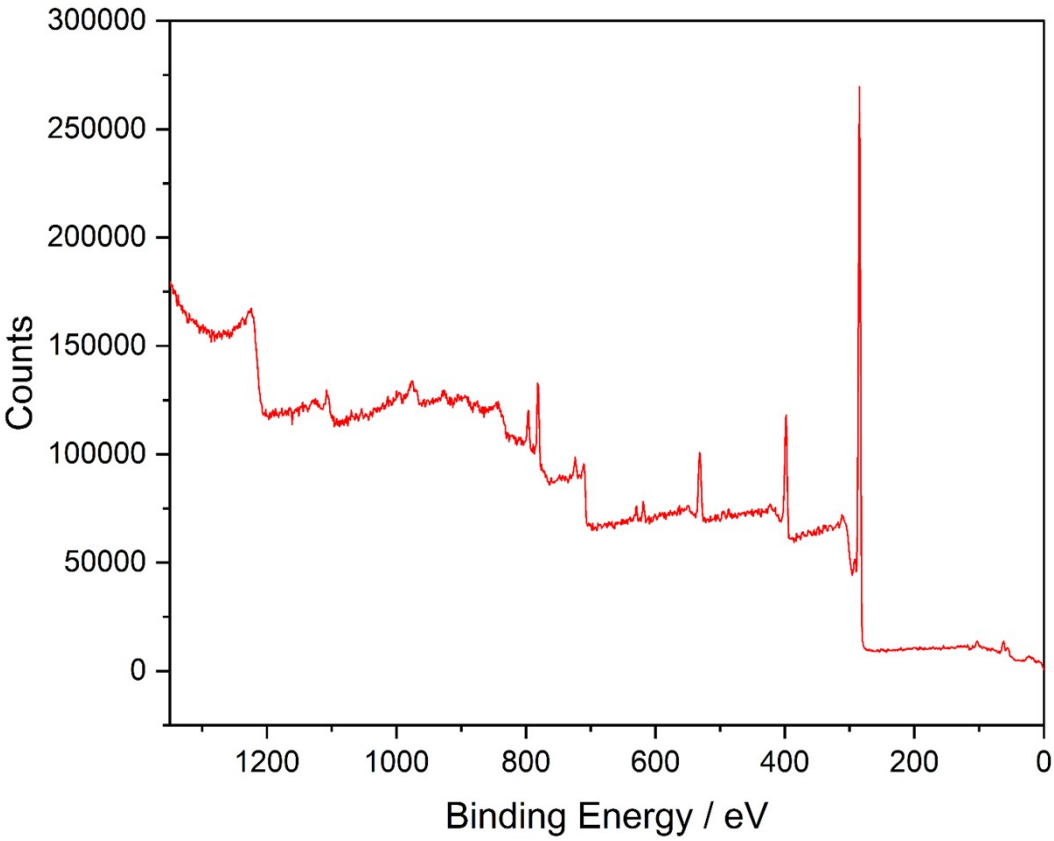

Figure S15. XPS full survey spectrum of **3**.

Table S7. XPS peak tables of **3**.

Name	Start BE	Peak BE	End BE	Height CPS	FWHM eV	Area (N)	Atomic %
C1s	297.85	284.78	279.85	48044.27	1.84	1.3	80.83
N1s	404.55	397.21	393.25	9064.63	2.47	0.19	11.9
O1s	536.85	530.63	523.55	4212.27	3.63	0.07	4.5
Fe2p1	736.9	722.88	719.2	1316.34	4.51	0.02	1.11
Co2p1	803.8	795.25	789.2	3326.67	2.16	0.02	1.23
I3d5	623.05	617.64	611.6	1305.41	1.88	0	0.17
Si2s	157.4	152.44	147.7	111.26	0.08	0	0.26

EDS Measurements

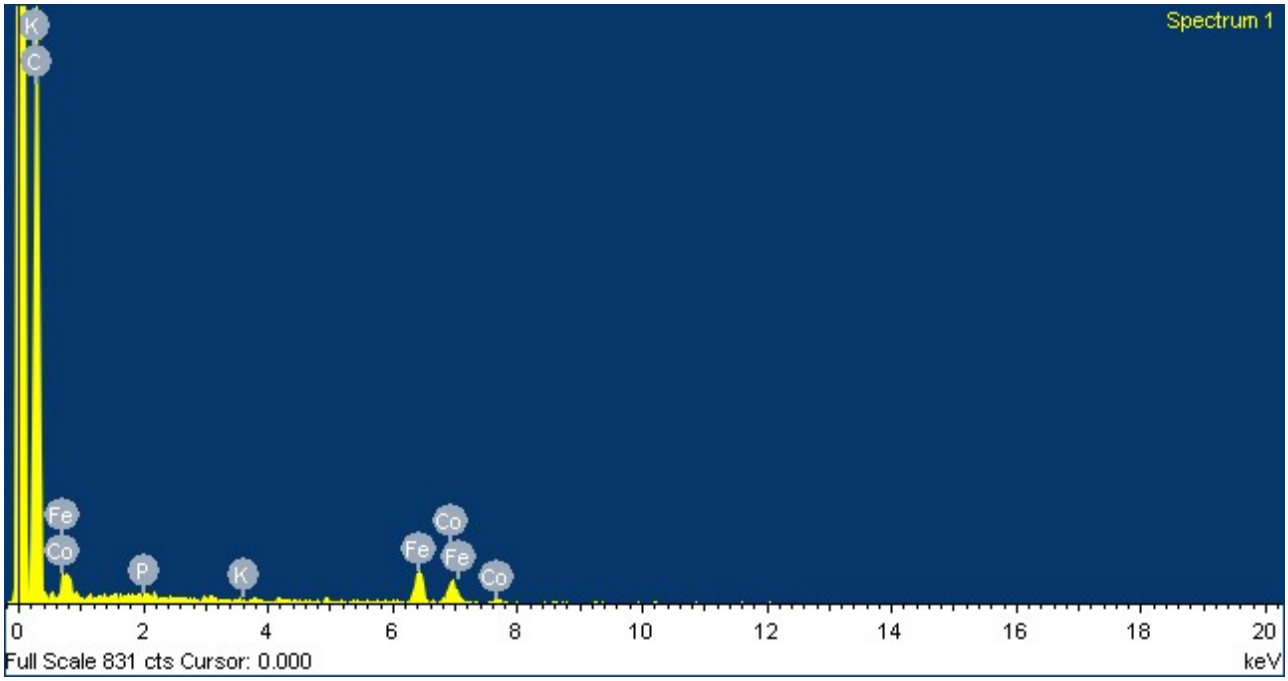

Figure S16. Energy dispersive x-ray spectrum of **3**.

Table S8. EDS elemental analysis results of **3**.

Element	Weight%	Atomic%
C	87.94	97.20
P	0.00	0.00
K	0.00	0.00
Fe	6.76	1.61
Co	5.30	1.19
Totals	100.00	

Mass spectrum

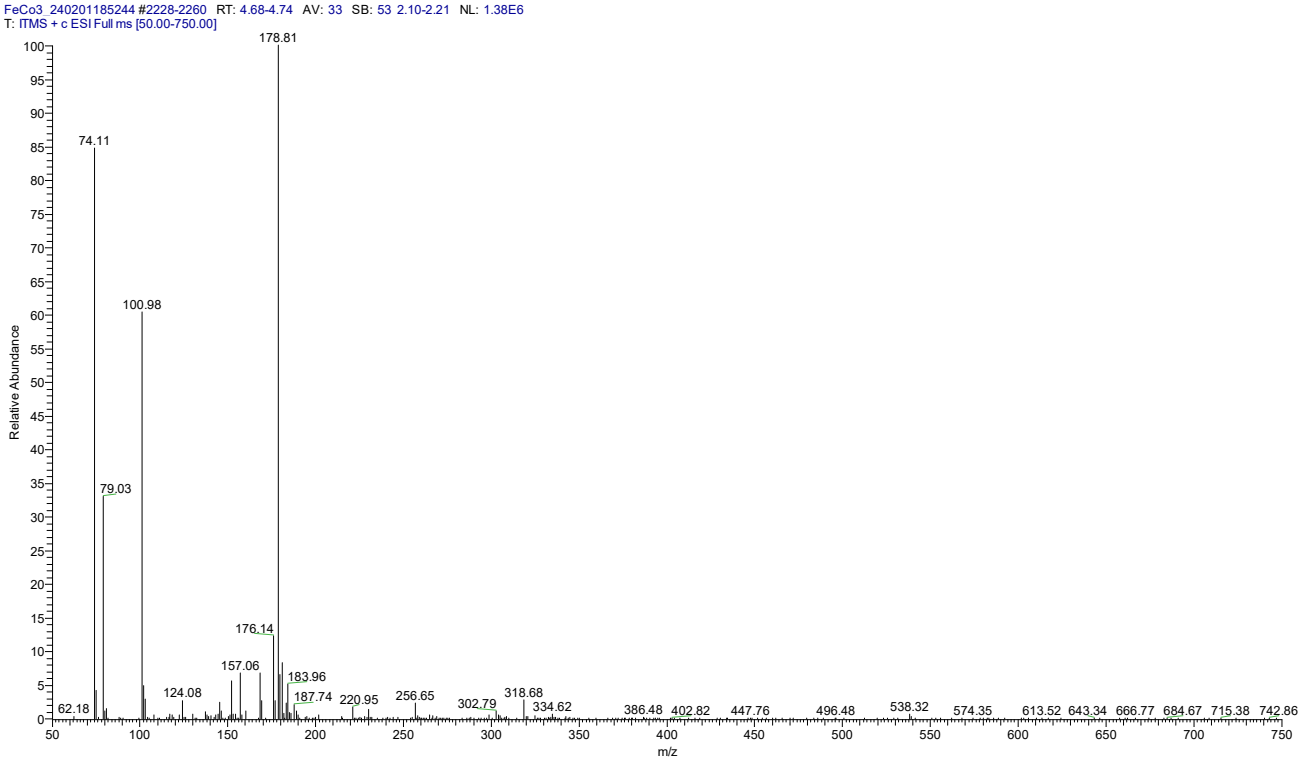

Figure S17. Electrospray mass spectrum of the DMSO digested sample of **3**. Complex **3** was immersed in acetone for a few hours and then heated at 330 K to removal the guests before mass spectrum experiment.

Table S9. Assignments of the principle peaks in the electrospray mass spectra of **3**.

Assignments	*m/z* (calc)
$[Et_2NH_2]^+$	74.10
$[DMSO+H]^+$	79.02
$[DMSO+Na]^+$	101.00
$[2DMSO+Na]^+$	179.02
$[PPN]^+$	538.18

Magnetization

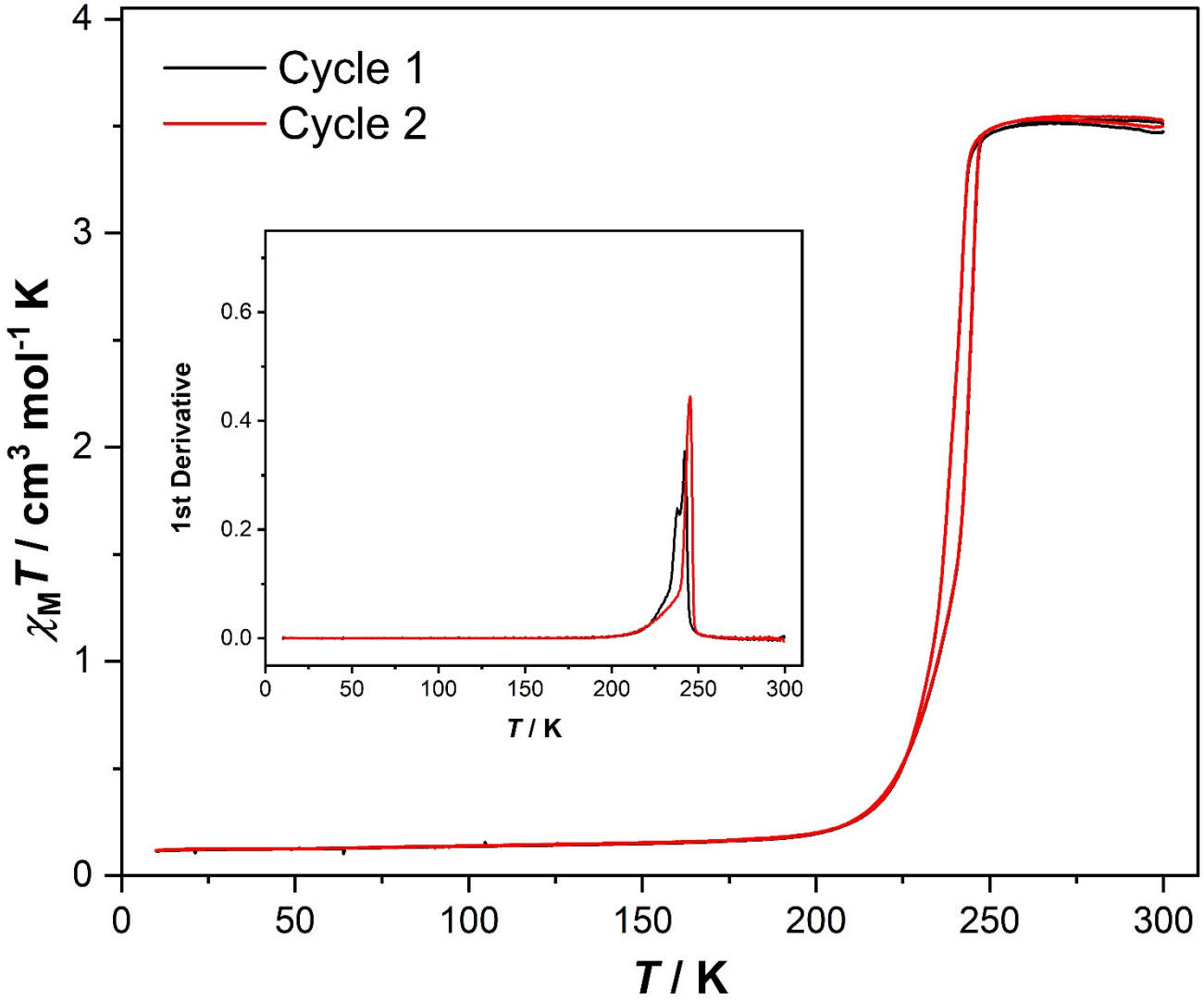

Figure S18 The temperature-dependent magnetic susceptibility data of **1** with a sweep rate of 2 K min^{-1}. The first derivative curve of magnetic data is shown in the inset.

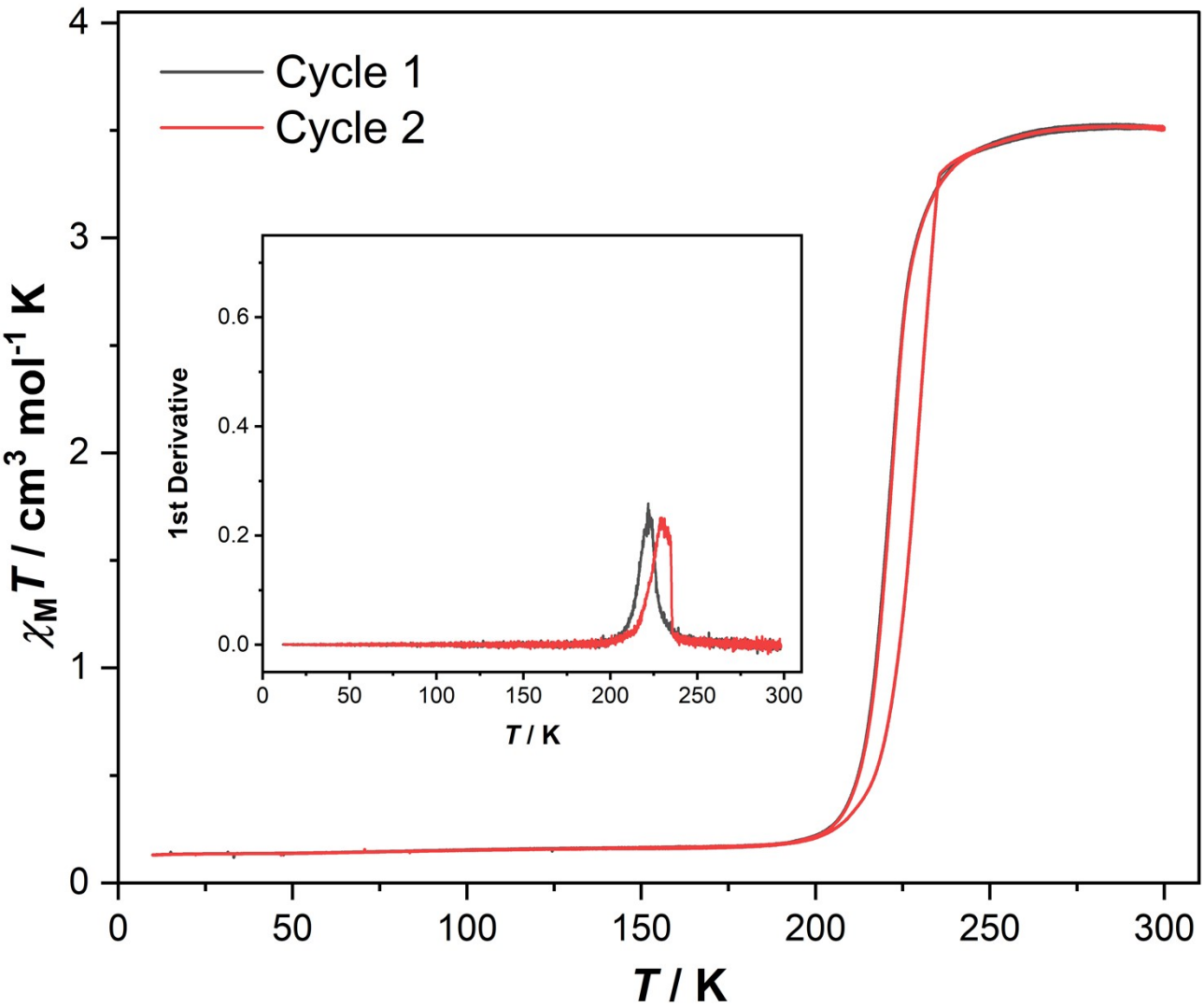

Figure S19. The temperature-dependent magnetic susceptibility data of **2** with a sweep rate of 2 K min^{-1}. The first derivative curve of magnetic data is shown in the inset.

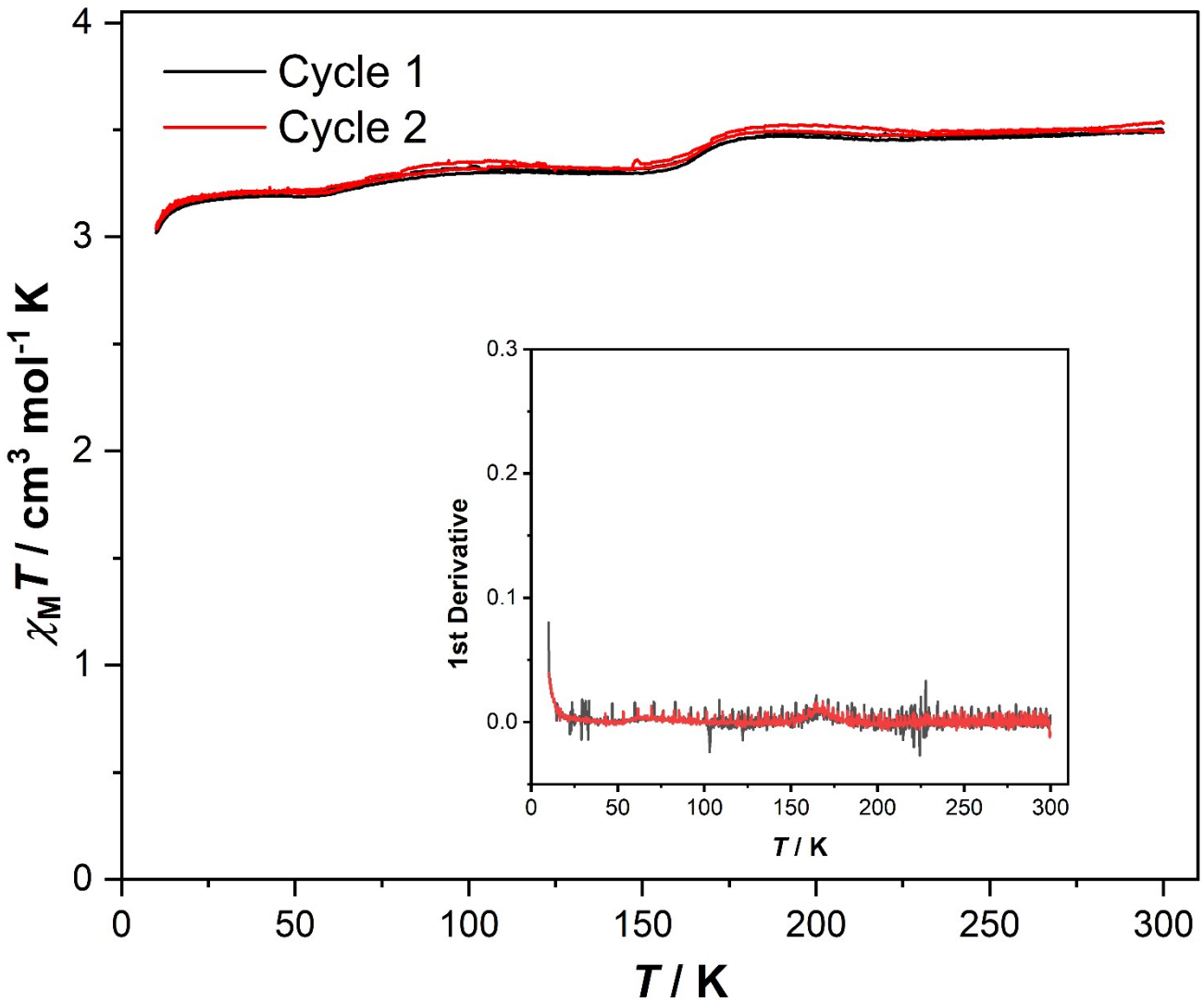

Figure S20. The temperature-dependent magnetic susceptibility data of **3** with a sweep rate of 2 K min^{-1}. The first derivative curve of magnetic data is shown in the inset.

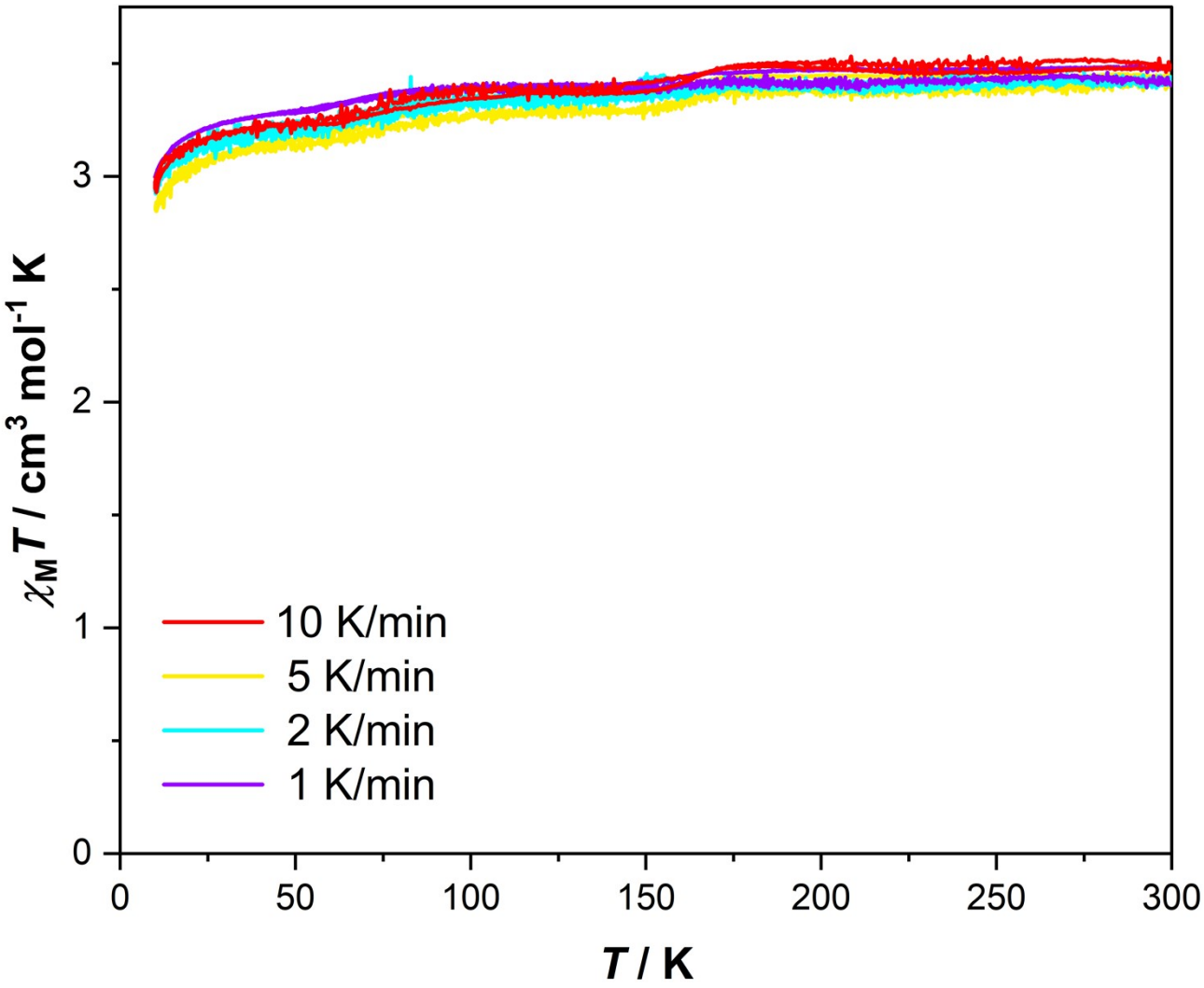

Figure S21. Variable-temperature magnetic susceptibility for **3** at different scan rate.

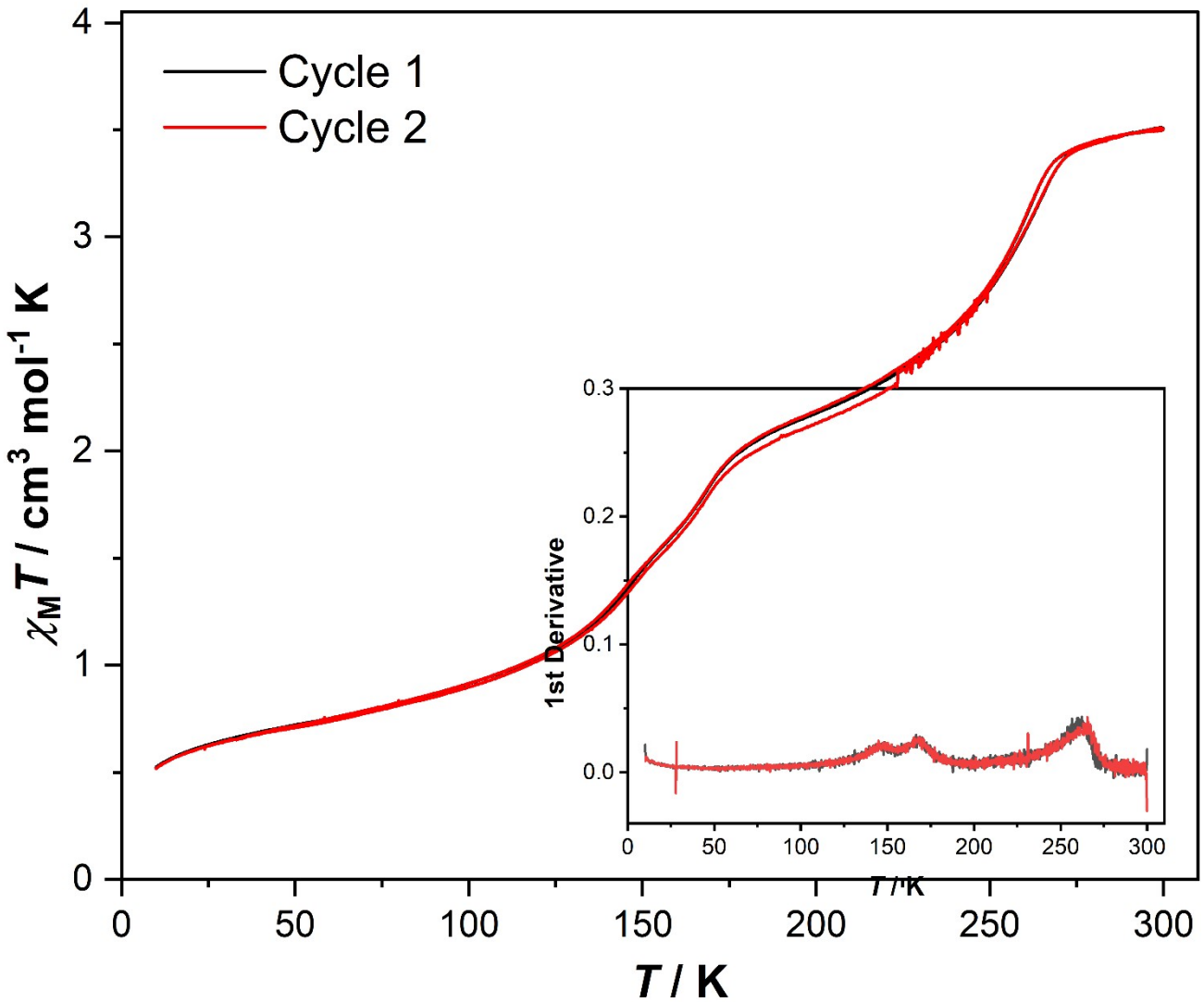

Figure S22. The temperature-dependent magnetic susceptibility data of **3**′ with a sweep rate of 2 K min^{-1}. The first derivative curve of magnetic data is shown in the inset.

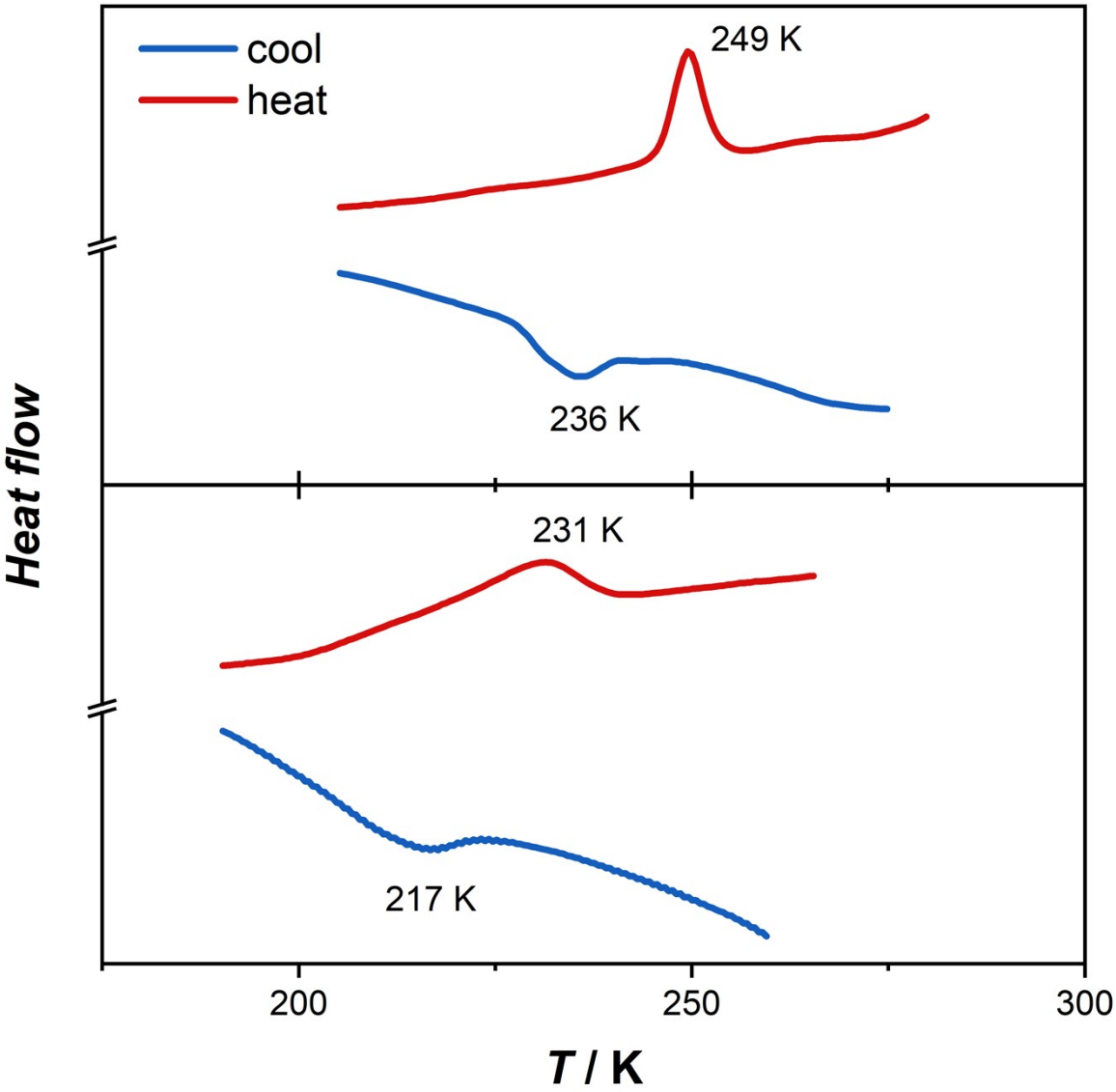

Figure S23. Differential scanning calorimetry measurements for **1** (up) and **2** (down) with a sweep rate of 10 K min^{-1}.

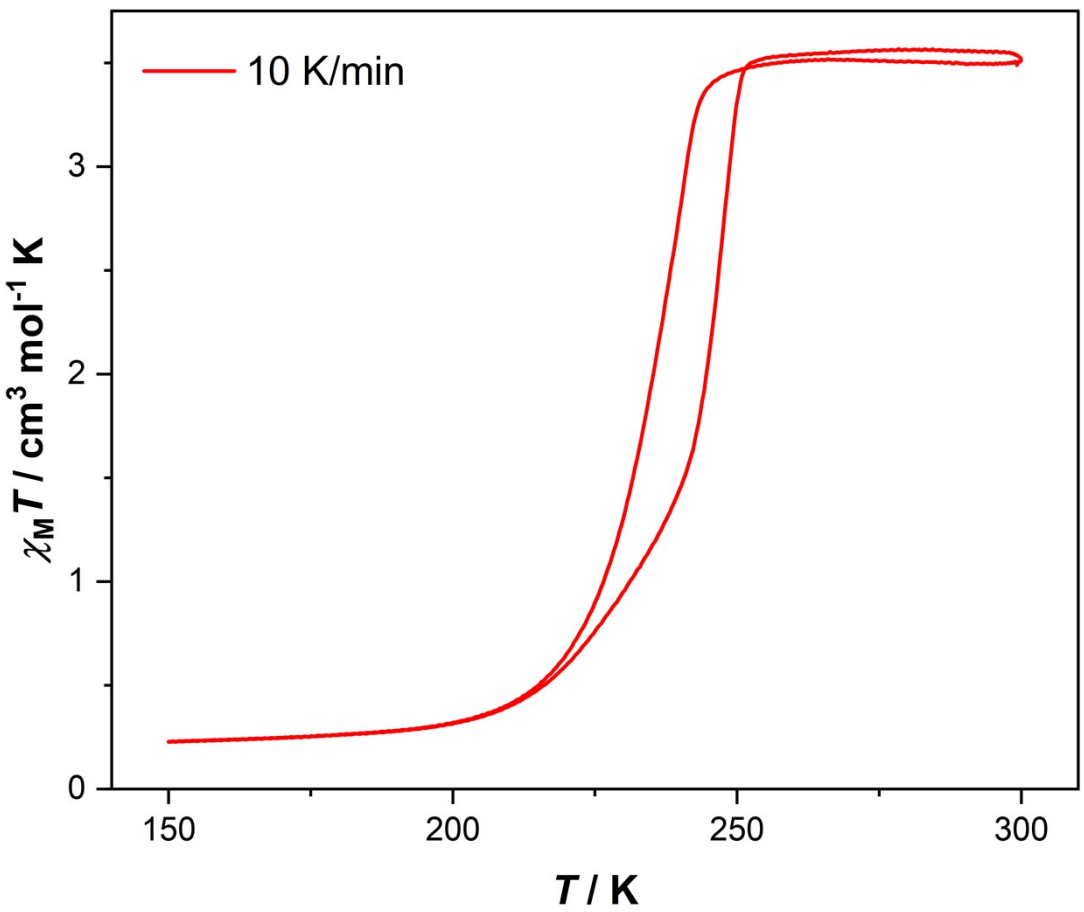

Figure S24. The temperature-dependent magnetic susceptibility data of **1** with a sweep rate of 10 K min^{-1}. The transition temperatures for the single-step SCO behavior are 234/244 K with a hysteresis of 10 K.

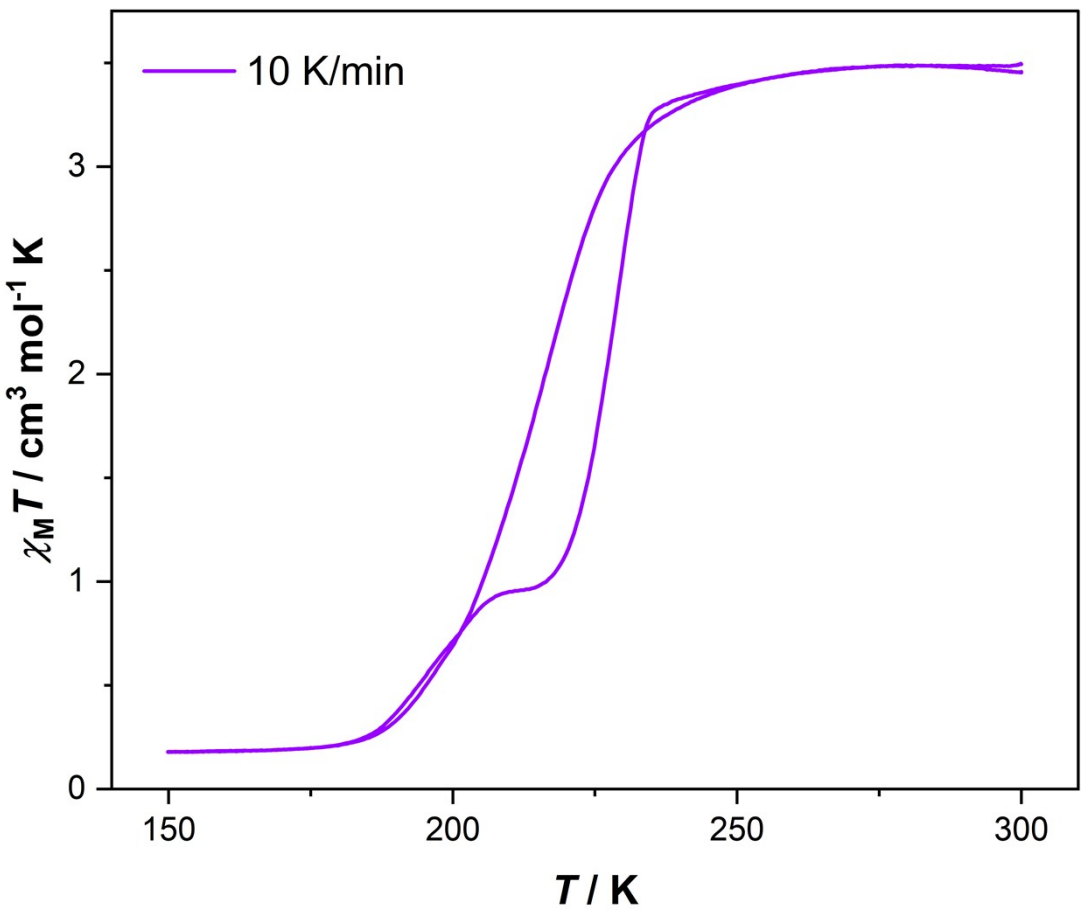

Figure S25. The temperature-dependent magnetic susceptibility data of **2** with a sweep rate of 10 K min^{-1}. The transition temperatures for the single-step SCO behavior are 214/226 K with a hysteresis of 12 K.

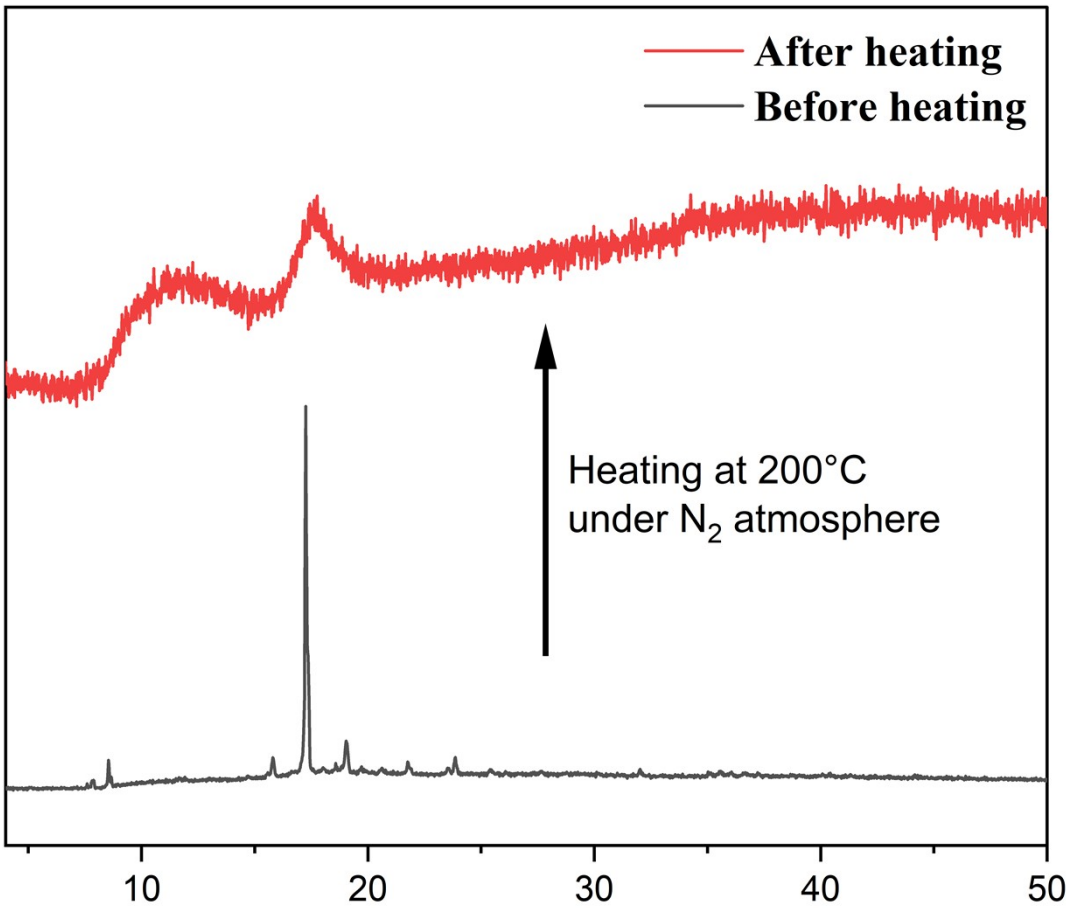

Figure S26. Powder X-ray diffraction (PXRD) patterns for **3** before and after heating. The empty framework collapsed as all the solvents escaped from the lattice.

Referrence

1 D. Pinkowicz, H. I. Southerland, C. Avendaño, A. Prosvirin, C. Sanders, W. Wernsdorfer, K. S. Pedersen, J. Dreiser, R. Clérac, J. Nehrkorn, G. G. Simeoni, A. Schnegg, K. Holldack and K. R. Dunbar, *J. Am. Chem. Soc.* 2015, **137**, 14406-14422.

2 G. Sheldrick, *Acta Cryst. A*. 2008, **64**, 112-122.

3 O. V. Dolomanov, L. J. Bourhis, R. J. Gildea, J. A. K. Howard and H. Puschmann, *J. Appl. Crystallogr.* 2009, **42**, 339-341.

4 G. Sheldrick, *Acta Cryst. C*. 2015, **71**, 3-8.